ELSEVIER

Journal of Atmospheric and Solar-Terrestrial Physics 69 (2007) 303–313

Journal of ATMOSPHERIC AND SOLAR-TERRESTRIAL PHYSICS

www.elsevier.com/locate/jastp

On the relationship of SAPS to storm-enhanced density

J.C. Foster[a,*], W. Rideout[a], B. Sandel[b], W.T. Forrester[b], F.J. Rich[c]

[a]*Massachusetts Institute of Technology, Haystack Observatory, Westford, MA, USA*
[b]*Lunar and Planetary Laboratory, University of Arizona, Tucson, AZ, USA*
[c]*Air Force Research Laboratory, Hanscom AFB, Ma,USA*

Received 25 April 2006; received in revised form 26 July 2006; accepted 27 July 2006
Available online 1 December 2006

Abstract

We use magnetic field-aligned mapping between the ionosphere and the magnetosphere to intercompare ground-based observations of storm enhanced density (SED), and plasmasphere drainage plumes imaged from space by the IMAGE EUV imager, with the enhanced inner-magnetosphere/ionosphere SAPS electric field which develops during large storms. We find that the inner edge of the SAPS electric field overlaps the erosion plume and that plume material is carried sunward in the SAPS overlap region. The two phenomena, SED in the ionosphere and the erosion plume at magnetospheric heights, define a common trajectory for sunward-propagating cold plasma fluxes in the midnight—dusk–postnoon sector. The SAPS channel at ionospheric heights and its projection into the equatorial plane serve to define the sharp outer boundary of the erosion plume. The SAPS electric field abuts and overlaps both the plasmasphere boundary layer and the plasmasphere erosion plume from pre-midnight through post-noon local times.

Keywords: Ionosphere; Plasmasphere; Electric field; *M-I* coupling; Subauroral

1. Introduction

1.1. Storm-enhanced density and the plasmasphere erosion plume

Recent studies highlighting the disturbance effects observed in the ionosphere and magnetosphere during geomagnetic disturbances and their space weather effects, have heightened interest in the processes occurring in the plasmasphere boundary layer (PBL) (Carpenter and Lemaire, 2004). Enhanced cold plasma total electron content (TEC) is observed at mid-latitudes, inside the PBL, in the post-noon beginning in the early phases of the storms, while D_{st} is falling (e.g. Tsurutani et al., 2004). At the poleward extent of this region, elevated TEC is carried sunward and poleward in plumes of storm-enhanced density (SED (Foster, 1993)). In the dusk sector where they are formed, the SED plumes are associated with the stripping away of the outer layers of the plasmasphere/ionosphere by the disturbance electric field. This process produces narrow plasmasphere drainage plumes (Sandel et al., 2001; Foster et al., 2002) of cold plasma which extend along magnetic-field lines between the plasmasphere and the ionosphere (e.g. Chi et al., 2005) and which are transported sunward (V∼ExB) in the disturbance electric field (Foster et al., 2004).

*Corresponding author. Tel.: +1 781 981 5621; fax: +1 781 981 15766.
E-mail address: jfoster@haystack.mit.edu (J.C. Foster).

1364-6826/$ - see front matter © 2006 Elsevier Ltd. All rights reserved.
doi:10.1016/j.jastp.2006.07.021

Following the original definition of SED as sunward-convecting cold plasma (Foster, 1993), we limit the use of this term to indicate that portion of the disturbance-enhanced TEC which is (or recently has been) entrained in the sunward convection within either the PBL (outer-plasmasphere field lines) or within the erosion plumes and their extension into the polar cap (Foster et al., 2005b). TEC enhancements in the equatorial anomalies or within the inner plasmasphere (e.g. Tsurutani et al., 2004; Mannucci et al., 2005; Foster and Rideout, 2005) are separate phenomena and are not addressed directly in the following discussion.

1.2. Previous studies of SAPS and their relationship to drainage plumes

The sub-auroral polarization stream (SAPS) electric field (Foster and Burke, 2002) refers to the region of enhanced poleward electric field which forms equatorward of electron precipitation in the dusk to midnight sector in disturbed conditions. SAPS forms as pressure gradients at the inner edge of the disturbance-enhanced ring current drive region 2 field-aligned currents into the evening-sector ionosphere. Large poleward-directed electric fields are set up to drive closure currents across the low-conductivity region equatorward of the auroral-electron precipitation. Observations of this phenomenon at ionospheric altitudes (Yeh et al., 1991; Foster and Burke, 2002; Foster and Vo, 2002) describe the occurrence characteristics and persistence of the SAPS electric field whose latitude extent spans the region between the electron-plasma sheet and the outer reaches of the plasmasphere (the PBL). Significant magnetospheric effects occur as the SAPS electric field maps along the field lines and is observed at higher altitudes (e.g. Rowland and Wygant, 1998).

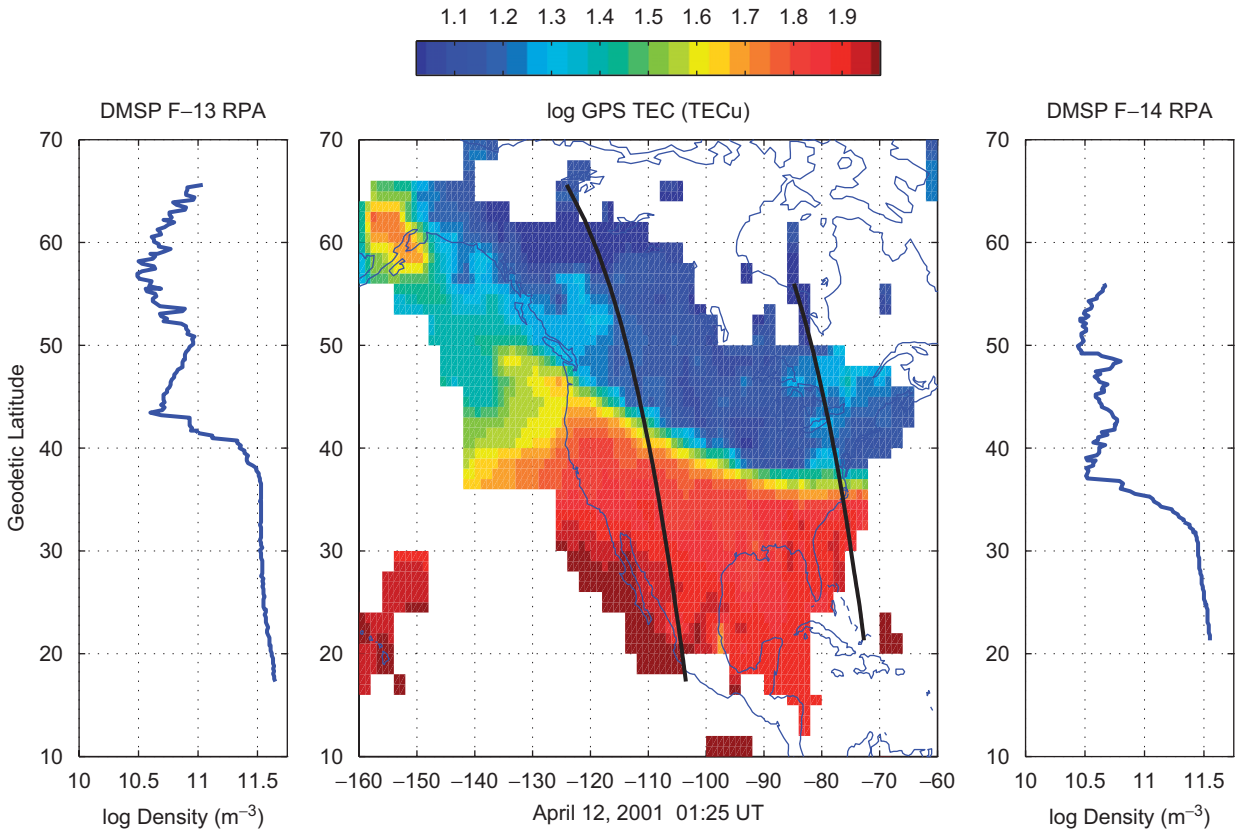

Fig. 1. Observations with a distributed array of GPS receivers show the perturbation of total electron content (TEC) over North America in the evening sector during the April 12, 2001 disturbance. A sharp boundary in TEC delineating the edge of the ionospheric trough cuts diagonally across the US mainland. Also shown are the ionospheric tracks of two DMSP satellites. Plots of in situ plasma density (RPA data at the ~830 km satellite altitude) are shown at either side of the TEC map.

Previous studies done at ionospheric F-region heights have indicated that the equatorward extent of the SAPS electric field overlaps the SED region in the outer PBL (Foster et al., 2002, 2004). Those studies combined sunward drift-velocity observations with the Millstone Hill radar and the DMSP satellites with observations of SED plumes made with GPS TEC. Foster et al. (2002) presented dipole magnetic-field projections of the boundaries of the low-altitude SED observations to the equatorial plane, where they compared closely with the location of plasmasphere erosion plumes seen with the IMAGE EUV instrument. This relationship suggests that the SAPS electric field maps along field lines between the ionosphere and the plasmasphere, overlapping flux tubes of cold plasma in the outer PBL in the midnight to dusk sector, resulting in sunward-streaming SED and plasmasphere erosion plumes in the post-noon sector.

In order to validate this hypothesis further, we project simultaneous IMAGE EUV observations of the configuration of the plasmasphere and observations of SED and plasma drift velocity observed at ionospheric heights to a common reference frame. Using a realistic magnetic field model (Tsyganenko, 2002), we map the Millstone Hill ISR, DMSP RPA and IDM topside observations, and IMAGE EUV data to the magnetospheric equatorial plane. The relationship of the simultaneously observed SAPS, SED, and erosion plumes then can be determined unequivocally.

2. Observations and discussion

GPS TEC imagery detailing the characteristics of the strong erosion plume, which formed during the April 11/12, 2001 geomagnetic disturbance has been presented by Foster et al. (2004). IMAGE EUV

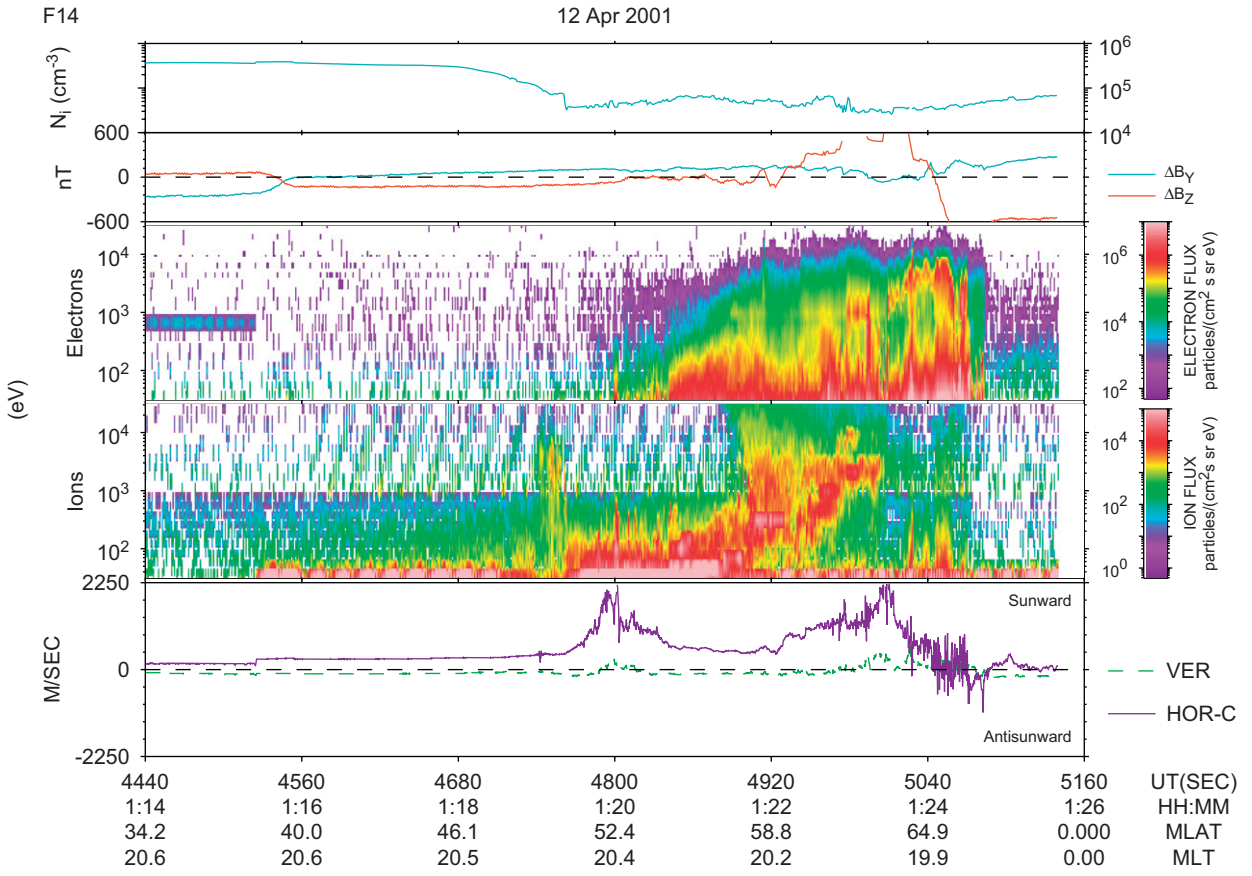

Fig. 2. DMSP F-14 observations of particles and fields are presented along the trajectory shown in Fig. 1. Across the sub-auroral region from the F-region density gradient (topmost panel, RPA density data) at ~01:19 UT to the equatorward boundary of precipitating electrons at ~01:21 UT (electron-flux spectrum, third panel from the top), a region of greatly enhanced cross-track plasma drift velocity (SAPS) was observed (centered at 01:20 UT, lower panel, ion-drift meter data).

plasmaspheric imagery was not available during the early strong phases of the event (see below), and we have chosen for detailed study an interval near 01:25 UT on April 12, 2001 for which we have simultaneous, GPS TEC, IMAGE EUV, Millstone Hill ISR, and DMSP overflight data.

Fig. 1 presents a snapshot of the distribution of TEC derived from observations with the distributed array of GPS receivers (cf. Coster et al., 2003). A sharp boundary between the higher TEC on field lines mapping into the PBL and the greatly reduced values of TEC in the ionospheric trough cuts diagonally across the US mainland. Whereas, the erosion plume at the height of this event (~19 UT Foster et al., 2004) was quite strong, at 01:25 UT a residual erosion plume follows this boundary and extends to the limit of the GPS field of view over Alaska. The ionospheric tracks of two DMSP overflights crossing the features seen from the ground by GPS are also shown in the figure. Plots of in situ plasma density (RPA data at the ~830 km satellite altitude) are shown at either side of the TEC map. Sharp topside density gradients (cf. Vo and Foster, 2001) are observed as the satellites fly poleward into the trough. Observations with the F14 satellite were made at a later local time (~20.5 MLT) while F13 crossed the boundary region near 16.5 MLT.

Fig. 2 presents detailed observations of particles and fields made along the DMSP F14 trajectory shown in Fig. 1. Across the sub-auroral region from the F-region density gradient (topmost panel, RPA density data) at ~01:19 UT to the equatorward boundary of precipitating electrons at ~01:21 UT (electron-flux spectrum, third panel from the top), a region of greatly enhanced cross-track plasma drift velocity was observed (centered at 01:20 UT, lower panel, ion-drift meter data). This is the region of the SAPS electric field (Foster and Burke, 2002). As is normally the case at this later local time (cf. Foster

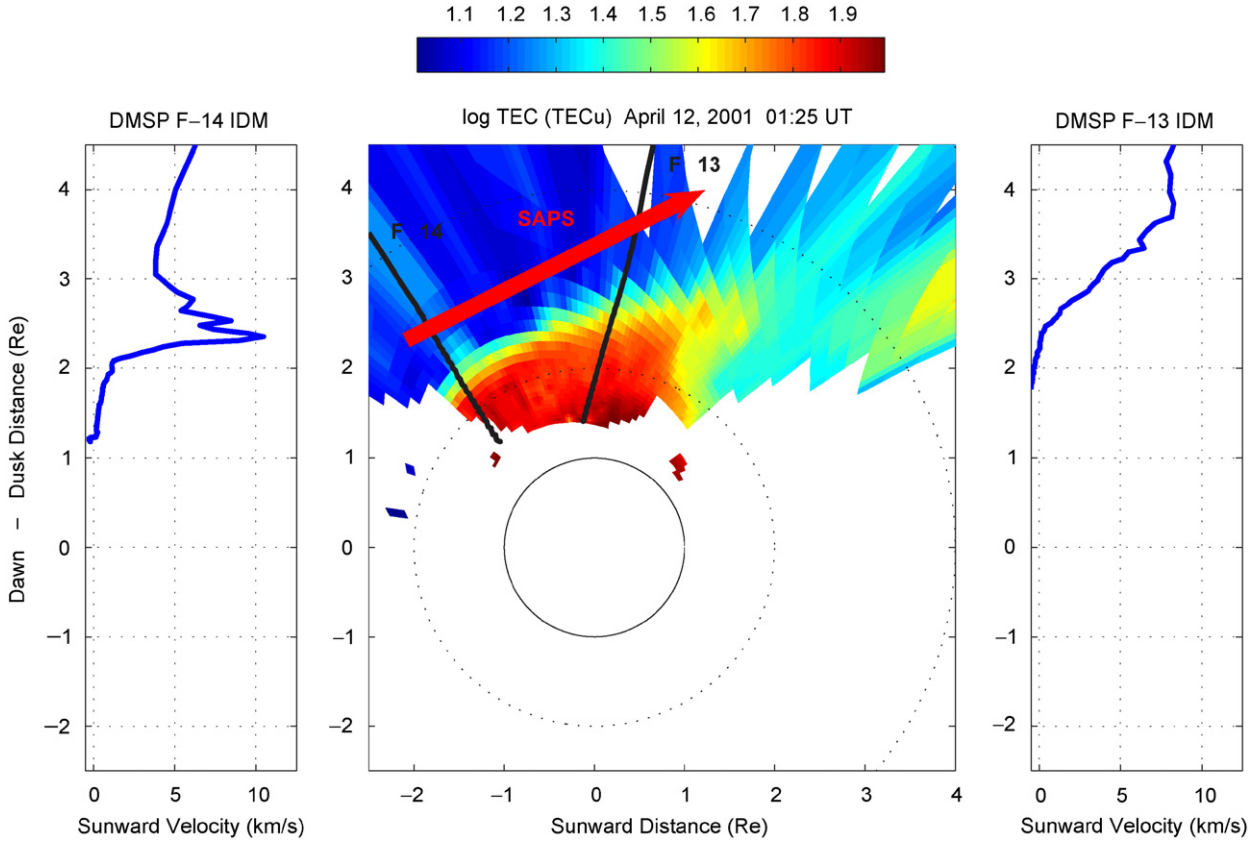

Fig. 3. The GPS TEC map of Fig. 1 is projected onto the GSM equatorial plane using field-aligned mapping in the disturbed geomagnetic field. DMSP drift meter velocities for F13 and F14 are projected similarly from their ~830 km observation altitude, and the resultant orbital tracks are shown on the figure. A straight line (red arrow) connects the points of peak SAPS velocity, indicating that the SAPS channel lies immediately outside, and parallels the magnetospheric projection of the SED and trough boundary.

and Vo, 2002), the SAPS electric field lies significantly equatorward and clearly separate from the region of two-cell sunward convection (seen in Fig. 2 from 01:22 to 01:24 UT). A burst of keV ions appears at the DMSP altitude at the inner edge of the SAPS at 01:19 UT, delineating the inward extent of plasmasheet ions to the vicinity of the PBL density gradient. Localized ion precipitation at the inner edge of the SAPS has been reported in previous studies (e.g. Foster et al., 1994).

2.1. SAPS in space

In Fig. 3 we project the GPS TEC map of Fig. 1 onto the geocentric solar magnetospheric (GSM) equatorial plane by mapping the 350 km altitude ionospheric penetration points to $Z_{GSM} = 0$ using the Tsyganenko (2002) magnetic field model calculated for the time of the observations. DMSP drift meter velocities for F13 and F14 (cf. Fig. 2) are projected similarly from their ~830 km observation altitude, and the resultant orbital tracks are shown in the figure. The magnitude of the horizontal drift velocity scales as E/B, such that the ~2 km/s ionospheric SAPS flow is increased to ~10 km/s in the equatorial plane, following the formulae of Mozer (1970). A red arrow is drawn connecting the positions of the SAPS flow-channel maxima on the two passes. The SAPS channel is seen to lie outside, and parallel to, the outer (later local time) edge of the projected SED erosion plume. At the earlier local time (F13 at 16.5 MLT) the inner extent of the SAPS flow overlaps the outer portions of the erosion plume, carrying the cold SED plasma sunward (see detailed discussion, below).

IMAGE EUV uses resonantly scattered sunlight from plasmaspheric helium to observe the structure and evolution of the PBL and the plasmapause across wide swaths of MLT (Sandel et al., 2001). The EUV instrument is sensitive to features where

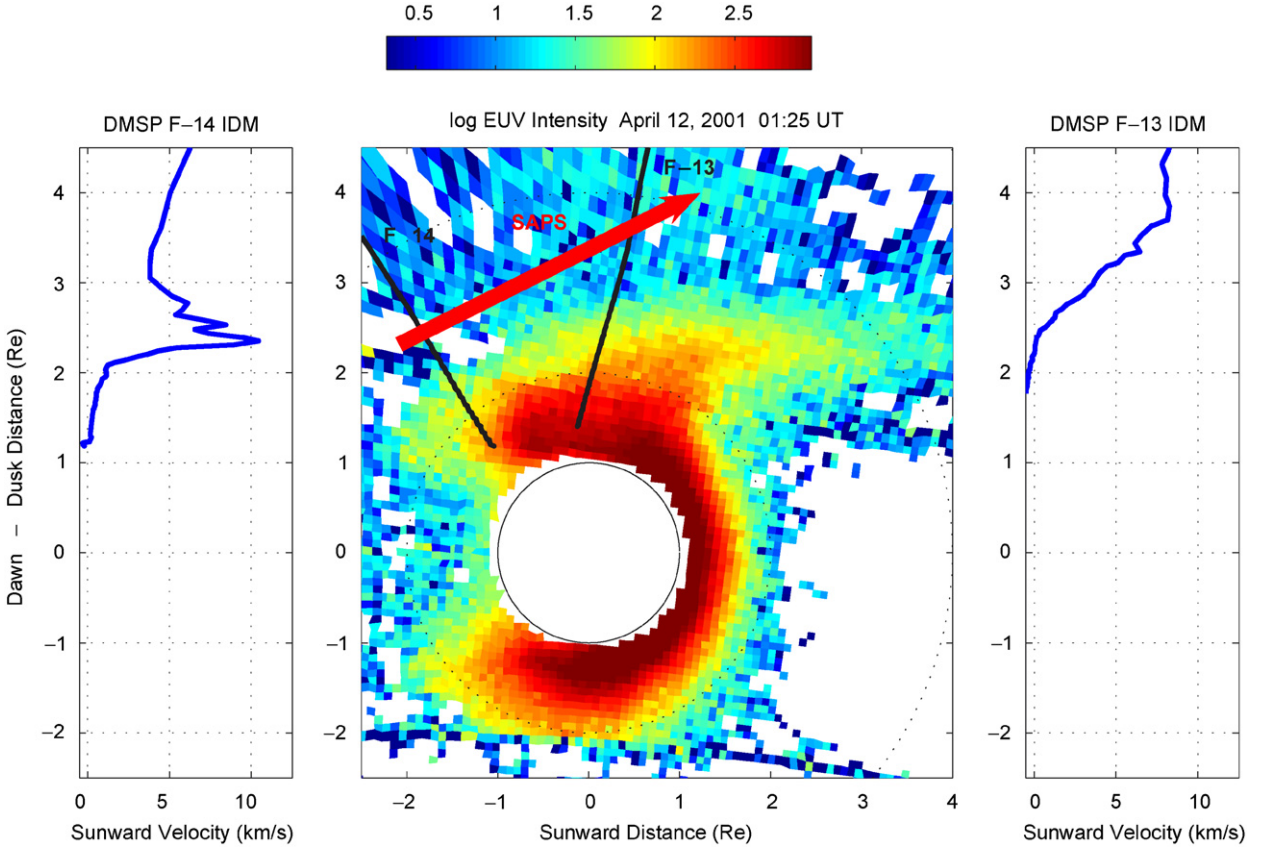

Fig. 4. An IMAGE EUV 'snapshot' of the plasmasphere and drainage plume at the time for the observations of Figs. 1–3 is mapped to the GSM equatorial plane using the Tsyganenko magnetic field mapping function. DMSP passes locate the SAPS channel immediately outside and adjacent to the plasmasphere drainage plume. The contours of the plasmasphere erosion plume viewed from space and of the SED plume viewed from the ground (cf. Fig. 3) are directly comparable and are seen to be strikingly similar.

the equatorial He+ abundance exceeds $\sim 40\,cm^{-3}$ (Goldstein et al., 2003). In Fig. 4 we relate the SAPS electric field channel seen at low altitude by DMSP to the plasmasphere erosion plume observed by the IMAGE space-based imager. We have taken the EUV 'snapshot' of the plasmasphere and drainage plume made at 01:23 UT and have mapped that image to the GSM equatorial plane using the Tsyganenko-mapping function. The EUV instrument records the line-of-sight integrated intensity as the instrument scans across the plasmasphere from its orbital vantage point above the Earth. The image displayed in Fig. 4 was mapped pixel-by-pixel by first determining the X, Y, Z GSM coordinates of the point of minimum L along the line of sight from the IMAGE spacecraft, computed using a dipole magnetic field. Each point was then mapped to GSM $Z = 0$ (the equatorial plane) using Tsyganenko mapping. A similar mapping of IMAGE EUV and DMSP observations to the GSM equatorial plane is presented by Lin et al. (2006) in discussing the October 31, 2003 event.

The contours of the plasmasphere erosion plume viewed from space (IMAGE EUV, Fig. 4) and of the SED plume viewed from the ground (GPS TEC, Fig. 3) are directly comparable and are seen to be strikingly similar. The sharp boundary of the ionospheric trough stretching across the US mainland seen in Fig. 1 is the low-altitude complement of the distinct outer edge of the erosion plume seen by IMAGE. The SAPS channel at ionospheric heights and its projection in the equatorial plane serve to define the sharp inner boundary of the trough and the outer boundary of the plume. It is the SAPS electric field which abuts and overlaps the PBL and the plasmasphere erosion plume from pre-midnight through post-noon local times. The red arrow in Figs. 3 and 4 denoting the center of the SAPS channel is drawn as a straight line, since its position was determined only at the two points defined by the DMSP orbits. It is reasonable to expect that the position of the outer boundary of the SED plume (Fig. 3) or the EUV erosion plume (Fig 4) maps along the position of the SAPS channel across the dusk sector.

In Fig. 5 we examine the overlap of the SAPS channel observed by DMSP F-13 with the erosion plume observed by IMAGE EUV. We plot the F-13 cross-track horizontal velocity in inertial coordinates projected to the GSM equatorial plane along the orbital track displayed in Fig. 4. Corotation velocity along this track is plotted as a dashed line and is eastward (negative) in inertial coordinates. The EUV intensity mapped to the GSM equatorial plane and displayed in Fig. 4 has been sampled along the DMSP orbital track. Log of EUV intensity (in relative units scaled and shifted to be displayed with the velocity data) is shown in Fig. 5. Four regions are delineated in the figure. In region I, corresponding to the inner plasmasphere inside $L \sim 1.6$, the plasma follows strict corotation, moving eastward in inertial coordinates. Outside of this, and extending out to radial distance of ~ 2.4 Re (region II), subrotation of the material in the inner plume is observed. In region III, extending out to 2.9 Re, the inner portion of the SAPS flow overlaps the outer reaches of the erosion plume. Outside ~ 2.6 Re (in region IIIa), the plume material has an overall westward (sunward) velocity. The main SAPS flow channel extends across region IV beyond the outer edge of the plume, where EUV count rates reach their background level. Peak flow in the SAPS channel is seen at ~ 3.7 Re along the F-13 orbital track. The data of Fig. 5 clearly show that the inner edge of the SAPS electric field overlaps the erosion plume and that plume material moves sunward in the SAPS overlap region.

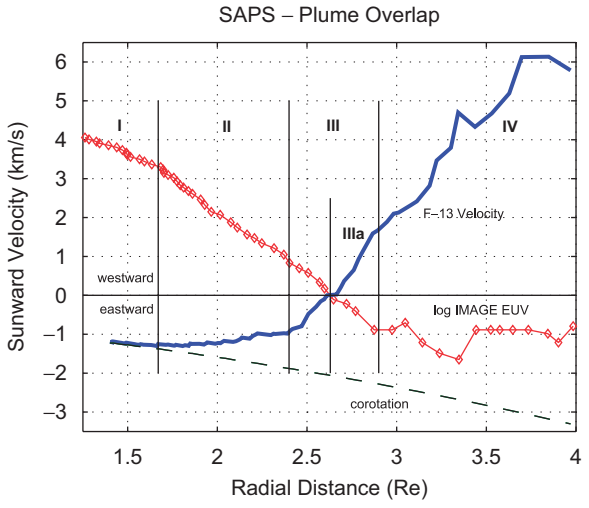

Fig. 5. F-13 cross-track horizontal velocity measured along the orbital track shown in Fig. 4 is presented in inertial coordinates (solid line). Corotation velocity along this track is shown as a dashed line. Log of EUV intensity (relative units) sampled along the DMSP orbital track is shown (diamonds). The inner portion of the SAPS convection channel overlaps the erosion plume carrying plume material sunward in the SAPS overlap region. See text for details.

2.2. SAPS and SED in the ionosphere

Foster et al. (2002, 2004) have demonstrated the relationship of the SED plume seen with GPS TEC and radar observations to the SAPS flow channel observed by DMSP at ionospheric heights. In those cases, the comparisons were made at a UT when the erosion plume is strongest over the continental US (when the central US is in the noon sector). At those times the DMSP passes were over the Atlantic Ocean, outside the TEC-map field of view. For the dusk local time of the event we analyze here (01:25 UT = 20.5 LT over the eastern USA), we recorded coincident ionospheric observations with the Millstone Hill incoherent scatter radar (ISR), GPS TEC, and the DMSP F-14 overflight discussed above. The Millstone Hill ISR, located near Boston, was making wide-area azimuth scans spanning a wide range of latitudes over eastern North America (e.g. Buonsanto et al., 1992). Ionospheric plasma density, velocity, and temperatures were recorded across a swath of latitude spanning the trough/plume boundary seen in Fig. 1.

In Fig. 6 we present the radar-density measurements for the time of the GPS TEC image of Fig. 1. Log density is shown and the sharp boundary of the electron density trough is seen near 37° geodetic latitude, coincident with the TEC boundary seen in Fig. 1. Strong returns seen between 45° and 55° latitude at ranges closest to the radar are contaminated by coherent backscatter from ionospheric turbulence in the region of strong auroral electric field. The path of the DMSP F-14 satellite is shown and the latitude variations of topside density (right panel) and sunward drift velocity (left panel) are shown. The DMSP velocity measurements display the clear double-peaked structure (Foster and Burke, 2002) associated with the SAPS electric field at lower latitude and the auroral two-cell convection region at latitudes between 45° and 55°. The SAPS convection channel aligns precisely with the deep ionospheric trough seen in the ISR data. At this

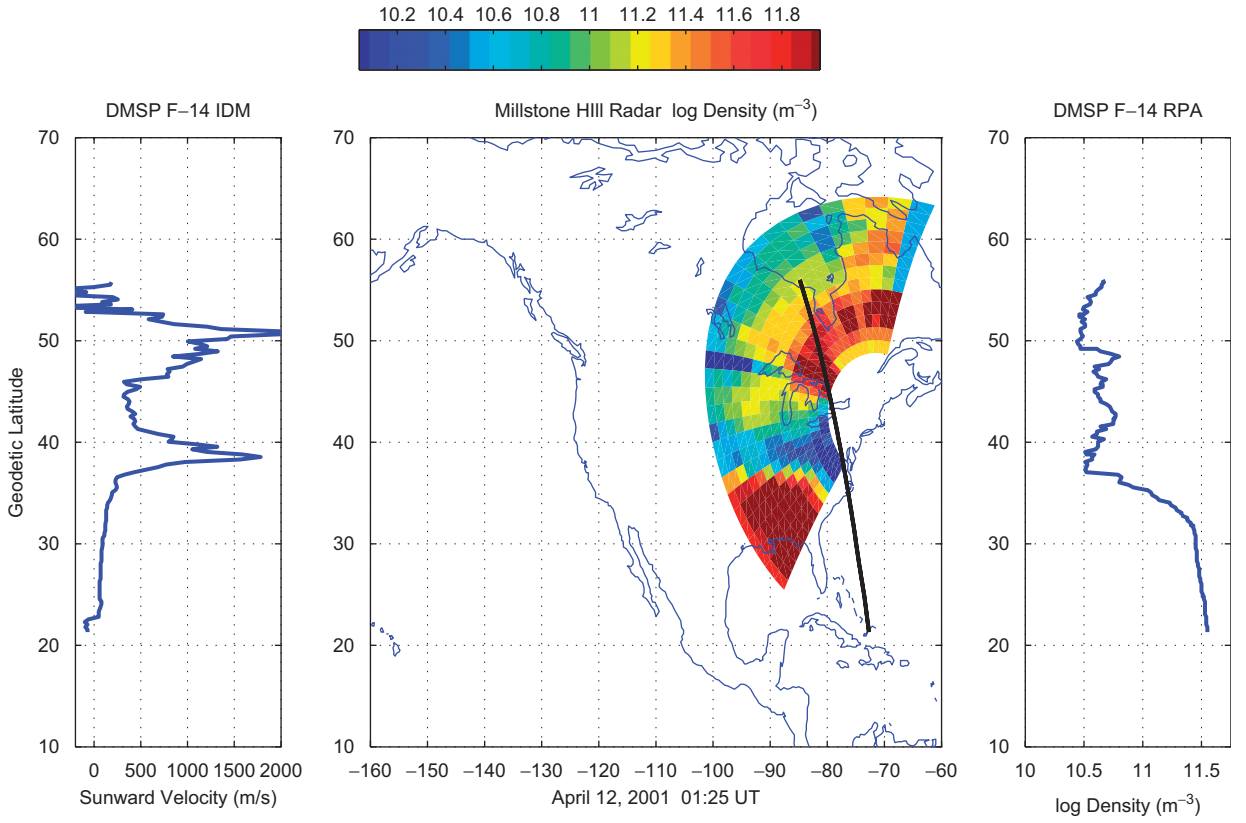

Fig. 6. Millstone Hill radar observations of F-region ionospheric density are shown for the time of the observations of Fig. 1. The path of the DMSP F-14 satellite is shown and the latitude variations of topside density (right panel) and sunward drift velocity (left panel) are shown (cf. Fig. 2). The SAPS convection channel centered near 39° latitude aligns precisely with the deep ionospheric trough seen in the ISR data.

time, late in the event when the intensity of the erosion plume was waning, the SAPS flow at 20.5 LT did not overlap significantly the region of high density/TEC plasma seen at lower latitudes. At local times nearer noon (see Fig. 5 and discussion), the inner edge of the SAPS flow overlapped the outer regions of the drainage plume.

2.3. May 30, 2003 event

The persistence of the SAPS electric field for many hours after the onset of an event (e.g. Foster and Vo, 2002) and the presence of long-lasting TEC enhancements in the low-latitude source region for the erosion plumes (e.g. Foster et al., 2005a), result in the type of late-event residual erosion plume presented in Fig. 1. A further example of this effect occurred at a similar LT (01:35 UT) during the May 30, 2003 event discussed in detail by Foster et al. (2005a) and Immel et al. (2005). During that event, as the dusk terminator advanced into the american sector, a pronounced enhancement of the TEC source region for the erosion plume formed over the Caribbean. As described in the earlier studies, this enhanced region then approximately corotated at a fixed longitude, with a continuing erosion plume drawn from its poleward limit. Foster and Coster (2006) discuss the repeated occurrence of such a TEC enhancement off the coast of Florida and in its magnetically conjugate region. These longitudinally confined enhancements of the source region for the erosion plume are associated with increasing

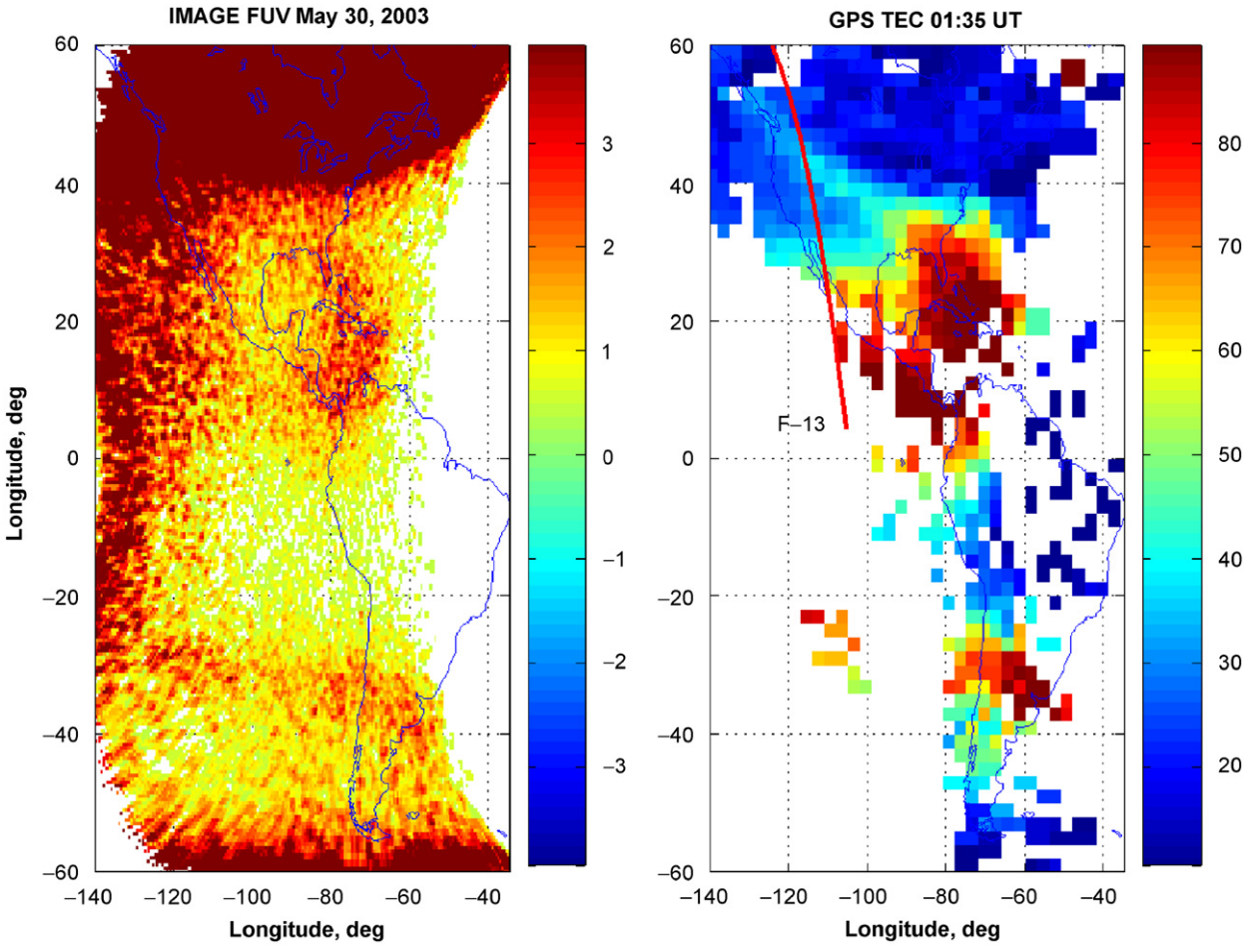

Fig. 7. Simultaneous IMAGE FUV (left) and GPS TEC (right) images of ionospheric perturbations during the May 30, 2003 storm for show a good one-to-one comparison of features and intensities. The bright patch seen by FUV over the Caribbean corresponds to the region of TEC enhancement at the base of the SED erosion plume. Bright FUV emissions at higher latitudes in the northern hemisphere indicate the equatorward extent of the aurora. An overflight of the DMSP F-13 satellite which crosses the erosion plume is indicated in red.

geomagnetic activity and the arrival of the sunset terminator in the vicinity of the south Atlantic magnetic anomaly.

Fig. 7, taken from Foster et al. (2005a), presents simultaneous IMAGE FUV (left) and GPS TEC (right) images at 01:35 UT for the May 30, 2003 event. The spectrographic imaging component of the FUV instrument (Mende et al., 2000) obtains simultaneous 2D images of terrestrial FUV emissions at wavelengths of 121.8 and 135.6 nm. The 135.6 nm channel, which detects OI emissions produced on the dayside, nightside, and at high latitudes by several processes, including the recombination of ionospheric $O+$ is shown here . This process is the dominant source of nightside FUV emissions away from the auroral oval. The intensity of the non-auroral emission is expected to be proportional to the total electron content along the line of sight. The relationship between the FUV and GPS TEC observations during this event has been presented by Immel et al. (2005).

The bright patch seen by FUV over the Caribbean corresponds to the region of TEC enhancement at the base of the SED erosion plume seen in the TEC image. Bright emissions at higher latitudes (above 40°) in the northern hemisphere indicate the equatorward extent of the aurora, and the narrow latitude extent of the equatorial anomaly (EA) crests is seen faintly (near 10°N and 30°S) to the west of the TEC and FUV enhancements. Scattered sunlight near the dusk terminator contaminated the western edge of the FUV images. The ionospheric footprint of an overflight of the DMSP F-13 satellite is indicated on the TEC frame. DMSP crosses the EA crest region near 10°N to the west of the TEC enhancement at the base of the SED plume, and then passes through the SED plume near 40°N at 110 W longitude.

Fig. 8 presents the in situ observations of density and cross-track velocity (positive westward; shown in inertial coordinates) observed by DMSP F-13. The equatorward extent of electron precipitation observed by the particle spectrometer (not shown) is

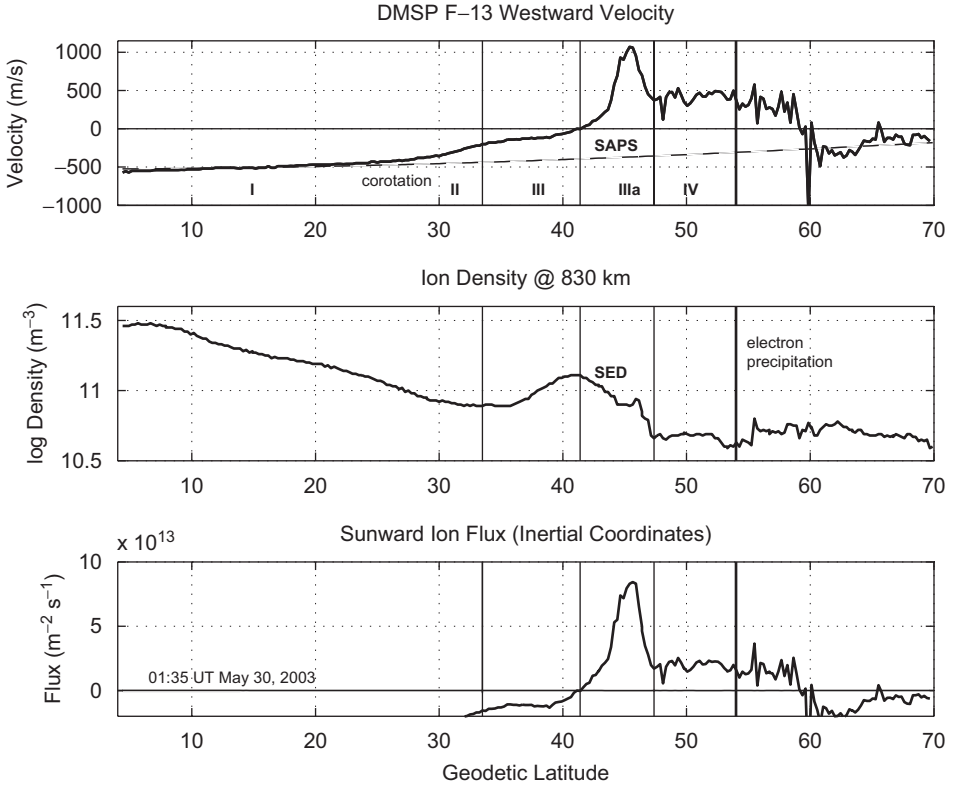

Fig. 8. DMSP F-13 observations of plasma density (middle panel) and cross-track velocity (top panel, positive westward) are shown. The equatorward limit of electron precipitation is indicated by vertical lines near 54°N. An extensive region of SAPS convection extends inward to $<35°$. The lower panel presents sunward ion flux calculated as the product of density velocity. The westward ion flux exceeds $8 \times 10^{13}\,m^{-2}\,s^{-1}$ in the topside F region (~830 km) in the outer portion of the SED plume.

indicated by vertical lines near 54°N. The extensive SAPS electric field extends equatorward from this point to ~30°N beyond which the plasma motion becomes purely corotational (region I). As done for the magnetospheric analysis of Fig. 5, the DMSP ionospheric passes across the SED and SAPS has been divided into four regions. The ionosphere begins to depart from corotation in region II and the SED plume (centered near 40°N) lies entirely within the extended region of SAPS electric field (region III). In region IIIa, the cold plasma of the SED is carried westward (towards earlier LT and noon). The lower panel presents the sunward ion flux calculated as the product of the density and velocity presented in the upper two panels. A peak sunward flux or 8×10^{13} ions $m^{-2} s^{-1}$ was observed where the strong SAPS/SAID (sub-auroral ion drifts) peak overlapped the outer region of the SED plume near 45°. The earlier study of Foster et al. (2004) found a similar value of sunward ion flux (5×10^{13} ions $m^{-2} s^{-1}$) in the SAPS overlap region for the April 11, 2001 event reported in that study. Sunward convection continued poleward of the SED plume, extending into the region of auroral electric precipitation poleward of 54°.

3. Summary

We have examined the relationship of the SAPS electric field channel to the cold-plasma erosion plumes at both magnetospheric and ionospheric heights. Field-aligned mapping has been used to display and intercompare the satellite and ground-based observations in a common reference plane. We find that the inner edge of the SAPS electric field overlaps the erosion plume and that plume material is carried sunward in the SAPS overlap region. The two phenomena, SED in the ionosphere and the erosion plume at magnetospheric heights, define a common trajectory for sunward-propagating cold-plasma fluxes in the midnight–dusk–postnoon sector. The SAPS channel at ionospheric heights and its projection into the equatorial plane serve to define the sharp outer boundary of the erosion plume.

Acknowledgments

GPS and IMAGE analysis have been supported by NASA SEC Guest Investigator Award (NAG5-12875) to the MIT Haystack Observatory. Radar observations and analysis at the Millstone Hill Observatory are supported by Co-operative Agreement ATM-0233230 between the National Science Foundation and the Massachusetts Institute of Technology. Work at The University of Arizona was funded by a subcontract from Southwest Research Institute, under NASA contract NAS5-96020 with SwRI. DMSP analysis is partially sponsored by the Air Force under Air Force Contract AF19628-00-C-0002. The authors acknowledge the support of A.J. Coster in developing GPS TEC analysis techniques.

References

Buonsanto, M.J., Foster, J.C., Sipler, D.P., 1992. Observations from millstone hill during the geomagnetic disturbances of March and April, 1990. J. Geophys. Res. 97, 1225–1243.

Carpenter, D.L., Lemaire, J., 2004. The plasmasphere boundary layer. Ann. Geophys. 22, 4291.

Chi, P.J., Russell, C.T., Foster, J.C., Moldwin, M.B., Engebretson, M.J., Mann, I.R., 2005. Density enhancement in the plasmasphere–ionosphere plasma during the 2003 Halloween magnetic storm: observations along the 265th meridian in North America. Geophys. Res. Lett. 32, L03S07, doi:10.1029/2004GL021722.

Coster, A.J., Foster, J., Erickson, P., 2003. Monitoring the ionosphere with GPS: space weather. GPS World 14 (5), 42–49.

Foster, J.C., 1993. Storm-time plasma transport at middle and high latitudes. J. Geophys. Res. 98, 1675–1689.

Foster, J.C., Burke, W.J., 2002. SAPS: a new characterization for sub-auroral electric fields. EOS 83, 393–394.

Foster, J.C., Coster, A.J., 2006. Localized stormtime enhancement of TEC at low latitudes in the American Sector. J. Atmos. Solar Terr. Phys. in press.

Foster, J.C., Rideout, W., 2005. Midlatitude TEC enhancements during the October 2003 superstorm. Geophys. Res. Lett. 32, L12S04.

Foster, J.C., Vo, H.B., 2002. Average characteristics and activity dependence of the subauroral polarization stream. J. Geophys. Res. 107 (A12), 1475.

Foster, J.C., Buonsanto, M.J., Mendillo, M., Nottingham, D., Rich, F.J., Denig, W., 1994. Coordinated stable auroral red arc observations: relationship to plasma convection. J. Geophys. Res. 99, 11429–11439.

Foster, J.C., Coster, A.J., Erickson, P.J., Goldstein, J., Rich, F.J., 2002. Ionospheric signatures of plasmaspheric tails. Geophys. Res. Lett. 29 (13).

Foster, J.C., Coster, A.J., Erickson, P.J., Rich, F.J., Sandel, B.R., 2004. Stormtime observations of the flux of plasmaspheric ions to the dayside cusp/magnetopause. Geophys. Res. Lett. 31, L08809.

Foster, J.C., Coster, A.J., Erickson, P.J., Rideout, W., Rich, F.J., Immel, T.J., Sandel, B.R., 2005a. Redistribution of the stormtime ionosphere and the formation of the plasmaspheric bulge, in inner magnetosphere interactions: new perspectives from imaging, In: J. Burch, M. Schultz, H. Spence (Eds.), Geophysical Monograph. ,vol. 159. American Geophysical Union, Washington DC pp. 277–289.

Foster, J.C., Coster, A.J., Erickson, P.J., Holt, J.M., Lind, F.D., Rideout, W., McCready, M., van Eyken, A., Greenwald, R.A., Rich, F.J., 2005b. Multiradar observations of the polar tongue of ionization. J. Geophys. Res. 110, A09S31.

Goldstein, J., Spasojevic, M., Reiff, P.H., Sandel, B.R., Forrester, W.T., Gallagher, D.L., Reinisch, B.W., 2003. Identifying the plasmapause in IMAGE EUV data using IMAGE RPI in situ steep density gradients. J. Geophys. Res. 108 (A4), 1147.

Immel, T.J., Foster, J.C., Coster, A.J., Frey, H.U., Mende, S.B., 2005. Global stormtime plasma redistribution imaged from the ground and space. Geophys. Res. Lett. 32 (3), L03808.

Lin, C.S., Yeh, H.-C., Sandel, B.R., Goldstein, J., Rich, F.J., Burke, W.R., Foster, J.C., 2006. Convection plasma drifts in the inner magnetosphere associated with a plasmaspheric drainage plume. J. Geophys. Res. submitted.

Mannucci, A.J., Tsurutani, B.T., Iijima, B., Komjathy, A., Wilson, B., Pi, X., Sparks, L., Hajj, G., Mandrake, L., Gonzales, W.D., Kozyra, J., Yumoto, K., Swisdak, M., Huba, J.D., Skoug, R., 2005. Hemispheric daytime response to intense solar wind forcing, in inner magnetosphere interactions: new perspectives from imaging, In: J. Burch, M. Schultz, H. Spence (Eds.),Geophysical Monograph vol. 159. American Geophysical Union, Washington DC pp 261-275.

Mende, S.B., et al., 2000. Far ultraviolet imaging from the IMAGE spacecraft. 3. Spectral imaging of Lyman-alpha and OI 135.6 nm. Space Sci. Rev. 91, 287–318.

Mozer, F.S., 1970. Electric field mapping in the ionosphere at the equatorial plane. Planet Sp. Sci. 18, 259.

Rowland, D.E., Wygant, J.R., 1998. Dependence of the large scale, inner magnetospheric electric field on geomagnetic activity. J. Geophys. Res. 103, 14959.

Sandel, B.R., King, R.A., Forrester, W.T., Gallagher, D.L., Broadfoot, A.L., Curtis, C.C., 2001. Initial results from the IMAGE extreme ultraviolet imager. Geophys. Res. Lett. 28, 1439.

Tsurutani, B.T., Mannucci, A., Iijima, B., Abdu, M.A., Sobral, J.H.A., Gonzalez, W., Guarnieri, F., Tsuda, T., Saito, A., Yumoto, K., Fejer, B., Fuller-Rowell, T.J., Kozyra, J., Foster, J.C., Coster, A., Vasyliunas, V.M., 2004. Global dayside ionospheric uplift and enhancement associated with interplanetary electric fields. J. Geophys. Res. 109, A08302.

Tsyganenko, N.A., 2002. A model of the near magnetosphere with a dawn–dusk asymmetry: 1. mathematical structure. J. Geophys. Res. 107 (A8).

Vo, H.B., Foster, J.C., 2001. A quantitative study of ionospheric density gradients at mid-latitudes. J. Geophys. Res. 106, 21555–21563.

Yeh, H.-C., Foster, J.C., Rich, F.J., Swider, W., 1991. Storm-time electric field penetration observed at mid-latitude. J. Geophys. Res. 96, 5707.